Decoupling of multiple antennas in terminals with chassis excitation using polarization diversity, angle diversity and current control

Li, Hui; Lau, Buon Kiong; Ying, Zhinong; He, Sailing

Published in:
IEEE Transactions on Antennas and Propagation

2012

Document Version:
Peer reviewed version (aka post-print)

Decoupling of Multiple Antennas in Terminals with Chassis Excitation Using Polarization Diversity, Angle Diversity and Current Control

Hui Li, *Student Member, IEEE,* Buon Kiong Lau, *Senior Member, IEEE,* Zhinong Ying, *Senior Member, IEEE,* and Sailing He, *Senior Member, IEEE*

***Abstract*—Excitation of the chassis enables single-antenna terminals to achieve good bandwidth and radiation performance, due to the entire chassis being utilized as the main radiator. In contrast, the same chassis excitation phenomenon complicates the design of multiple antennas for MIMO applications, since the same characteristic mode of the chassis may be effectively excited by more than one antenna, leading to strong mutual coupling and severe MIMO performance degradation. In this paper, we introduce a design concept for MIMO antennas to mitigate the chassis-induced mutual coupling, which is especially relevant for frequency bands below 1 GHz. We illustrate the design concept on a dual-antenna terminal at 0.93 GHz, where a folded monopole at one chassis edge excites the chassis' fundamental electric dipole mode and a coupled loop at the other chassis edge excites its own fundamental magnetic dipole mode. Since the two radiation modes are nearly orthogonal to each other, an isolation of over 30 dB is achieved. Moreover, we show that the antenna system can be conveniently modified for multiband operation, such as in the 900/1800/2600 MHz bands. Furthermore, by controlling the phase of the feed current on the folded monopole, the two antennas can be co-located on the same chassis edge with an isolation of over 20 dB. The co-located dual antenna prototype was fabricated and verified in the measurements.**

***Index Terms*— Antenna array, mutual coupling, MIMO systems, mobile communication.**

I. Introduction

High transmission rates of next generation communication systems require significant attention on antenna design [1]. Implementing multiple antennas in both base stations and terminals is a key solution to increase channel capacity without sacrificing additional frequency spectrum and transmit power. In reality, the compactness of today's terminals complicates the design of multiple antennas, since it results in strong mutual coupling and degradation in the expected performance of the antennas, such as bandwidth, efficiency and channel capacity [2]-[5].

Most of the existing coupling reduction techniques suitable for mobile terminals focus on relatively high frequency bands, including WLAN, DCS1800 and UMTS bands [6]-[10], even though in practice the problem of coupling is more severe at lower frequencies. Existing literature shows that the isolation of multiple antennas in compact terminals is typically less than 6 dB for frequencies below 1 GHz (see e.g., [11]). According to [12], decoupling at low frequency bands is challenging, because the chassis does not only function as a ground plane, but also as a radiator shared by the multiple antennas. Thus, the radiation patterns are strongly influenced by the shared chassis, such that angle and polarization diversities are difficult to achieve among the antennas for the purpose of decoupling. To avoid the excitation of the shared chassis by more than one antenna in a two-antenna setup, the position of the second antenna can be optimized to effectively reduce the chassis excitation [12]. In particular, the isolation is enhanced from below 4 dB to 10 dB, as the second antenna is moved from the edge of the chassis towards the center position, and the first antenna is kept at the other edge of the chassis. However, this technique is aimed at mitigating chassis excitation and does not create much angle and polarization diversities, which puts a limit on the achievable isolation. Furthermore, it is often impractical to place an antenna at the center of the chassis, considering the common layout of device components on the printed circuit board (PCB).

In this paper, based on the characteristic mode analysis in [12], a new concept is proposed to effectively mitigate coupling, especially chassis-induced coupling, among MIMO antennas. Instead of moving the second antenna from the chassis edge to the chassis center as in [12], we replaced the antenna at the chassis edge with a magnetic antenna to circumvent coupling with the first antenna, which intentionally excites the chassis. In this manner, we achieve both polarization and angle diversities. The concept is first demonstrated through an ideal flat dipole and a small loop. As one practical realization of the concept, we introduced a dual-antenna structure at 0.93 GHz, which consists of a folded monopole and a coupled feed loop on opposite edges of a chassis. The monopole excites the chassis, and radiates like

Manuscript received November 11, 2011. This work was supported in part by VINNOVA under grant no. 2009-04047 and 2008-00970, and also in part by a scholarship within EU Erasmus Mundus External Cooperation Window Lot 14.This paper was presented in part at the XXX URSI General Assembly and Scientific Symposium, Istanbul, Turkey, Aug 13-20, 2011, and submitted in part as a patent application with Sony Ericsson Mobile Communication AB.

H. Li and S. He are with the School of Electromagnetic Engineering, Royal Institute of Technology, SE-100 44 Stockholm, Sweden (e-mail: {huili, sailing} @ee.kth.se). They are also with the Center for Optical and Electromagnetic Research, Zhejiang University, Hangzhou, 310058, China.

B. K. Lau is with the Department of Electrical and Information Technology, Lund University, 221 00 Lund, Sweden (e-mail: Buon_Kiong.Lau@eit.lth. se).

Z. Ying is with Research and Technology, Corporate Technology Office, Sony Ericsson Mobile Communications AB, 221 88 Lund, Sweden (e-mail: Ying.Zhinong@sonyericsson.com).

a flat electric dipole. The coupled loop avoids exciting the chassis by radiating like a magnetic dipole at the point where the characteristic mode of chassis has the least magnetic field component. This approach effectively mitigates the chassis induced coupling and produces near-orthogonal radiation patterns, leading to both high isolation and high total antenna efficiencies. It should be noted that perfect orthogonal radiation patterns are only achieved by an infinitesimal dipole and an infinitesimal loop, since these ideal antenna patterns are orthogonally polarized. This phenomenon can also be understood in that, in the near field region, an infinitesimal dipole radiates pure electric field, whereas an infinitesimal loop yields pure magnetic field. Furthermore, the antenna design in this paper is based on the typical candybar-type mobile chassis, with the size of 100 mm × 40 mm. One can easily apply the proposed design principle by appropriate scaling to smart phones (e.g., 125 mm × 65 mm) for the 700 MHz LTE band. Alternatively, a larger bandwidth can be achieved with a larger chassis at the same operating frequency of 0.93 GHz.

The paper is organized as follows: In Section II, the radiation properties of a lossless dual-antenna structure (with an electric dipole and a small loop) are carefully analyzed in the context of applying the theory of characteristic mode to compact dual-antenna design. The design principle is then applied in Section III to obtain an efficient two-antenna solution for a compact chassis at 0.93 GHz. A varactor diode is applied to the coupled loop to tune its frequency and cover a larger bandwidth from 780 MHz to 980 MHz. Moreover, to establish multiband capability, we showed that the dual-antenna system can be slightly modified to operate in three bands, including the 900 MHz, 1.8 GHz and 2.6 GHz bands. Section IV demonstrates how the two antennas can be re-designed to be co-located on the same edge of the chassis, which greatly reduces the implementation space. A prototype of the co-located antenna system was fabricated, and the measured results are presented in Section V. Section VI concludes the paper.

II. Electric and Magnetic Dipole Antennas

Since the proposed design concept in this paper is based on exploiting the radiation characteristics of electric and magnetic dipole antennas, we begin by showing how these simple antenna structures are relevant to compact terminal applications, where all antenna elements are implemented on a small chassis.

In essence, a flat electric dipole antenna can be formed by appropriately exciting the entire chassis with an antenna element [13]. To illustrate the mechanism of chassis excitation, we used the theory of characteristic mode [14] to calculate the characteristic electric and magnetic fields of the chassis. For a 100 mm × 40 mm chassis, the normalized characteristic electric and magnetic fields on a plane 5 mm above the chassis at the first characteristic frequency (1.35 GHz) are shown in Figs. 1(a) and 1(b), respectively. Here, the chassis is modeled by a perfect conducting board. Fig. 1(a) reveals that, in order to strongly excite the first characteristic mode of the chassis, the antenna element should store electric energy in the near field (henceforth called 'electric antenna') and be placed at either of the two shorter edges of the chassis. Therefore, if two electric antennas are placed at the two chassis edges, both antennas will share the chassis as their radiator, causing severe mutual coupling.

On the contrary, according to Fig. 1(b), if an antenna at a shorter edge stores mainly magnetic energy but little electric energy (henceforth called 'magnetic antenna') in the near field, the antenna is unable to excite the chassis. This implies that if an electric antenna is used at the other edge to excite the chassis, the magnetic antenna will be unaffected by the chassis excitation, resulting in high isolation.

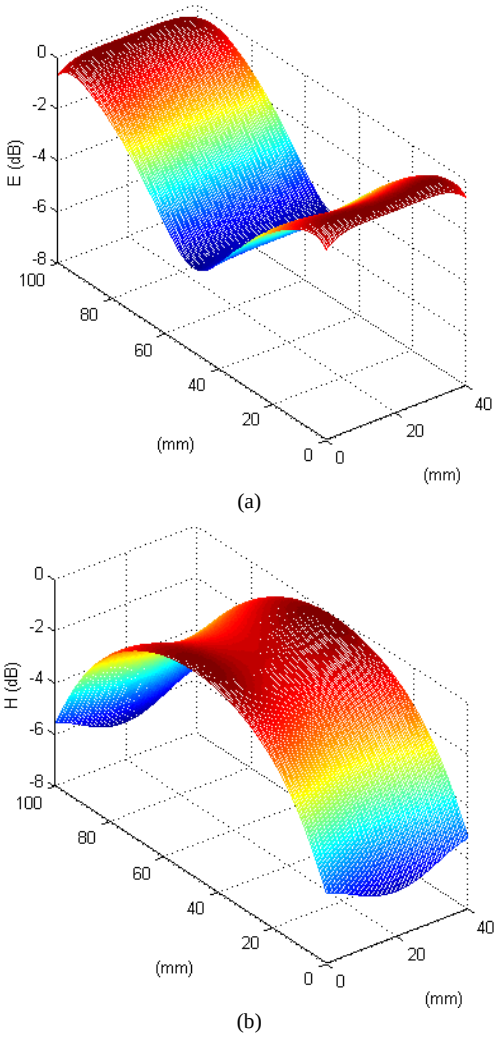

Fig. 1. The normalized magnitude of (a) the total electric field and (b) the total magnetic field for the characteristic mode of the chassis at 1.35 GHz.

To study the coupling performance of such an ideal dual-antenna setup, with an electric antenna perfectly exciting the chassis and a magnetic antenna avoiding chassis excitation, we utilized the equivalent dual-antenna structure in Fig. 2(a). Detailed geometries of the antenna structure are provided in Fig. 2(a). As can be seen, the whole structure retains the original chassis size of 100 mm × 40 mm. The dual antenna system consists of a flat dipole and a small loop, where the flat dipole models the excited chassis, and the small loop works as a magnetic antenna.

To realize the magnetic antenna with the small loop, we set the radius of the small loop to be 6.5 mm, corresponding to 0.018λ at 0.9 GHz. This ensures almost uniform in-phase

current distribution along the perimeter of the loop. The flat dipole is excited by a voltage applied at its normal feed point. Both antennas are assumed to be perfect electric conductors (PECs) and they are printed on a lossless substrate with the dielectric permittivity of 2.45 and the thickness of 0.8 mm.

Full-wave antenna simulations were carried out in the frequency domain using CST Microwave Studio. Both the flat dipole and the small loop resonate at 0.9 GHz, as shown by the scattering (or S) parameters in Fig. 2(b). Ideal single-stub matching networks [15] are used to ensure good impedance matching at the center frequency (with S_{11} < -20 dB). The total efficiencies of both antennas are 99% at 0.9 GHz, since the whole antenna system is assumed to be lossless. The isolation is above 25 dB, despite their close proximity to each other.

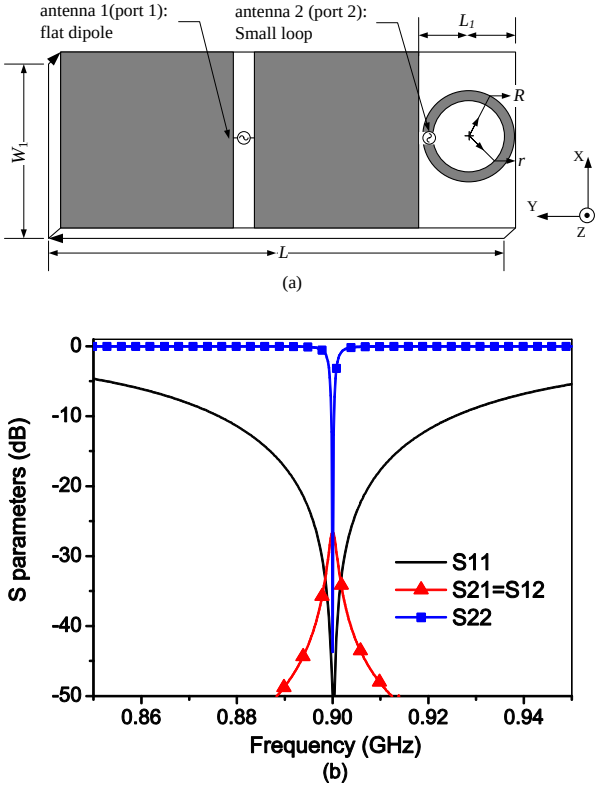

Fig. 2. (a) The geometries of the flat dipole and the small loop. The dimensions are: L = 100 mm, W_1= 40 mm, r = 6 mm, R = 7 mm, L_1 = 15 mm. (b) The S parameters of the ideal flat dipole and the small loop.

The *E*-theta and *E*-phi components of the normalized far-field antenna patterns at 0.9 GHz are presented in Fig. 3. The pattern of each antenna was obtained with the other antenna terminated in 50 Ω. Several observations can be made from the figure. Firstly, the flat dipole has a linearly polarized "donut" radiation pattern, which is similar to that of a conventional half wavelength dipole oriented along the *y* axis. Secondly, the small loop has the same "donut" radiation pattern as the magnetic dipole, with the peak gain along the plane of the loop and the *E*-phi component being 20 dB larger than the *E*-theta component. Comparing the *E*-phi components in Figs. 3(a) and 3(c) and the *E*-theta components in Figs. 3(b) and 3(d), it can be seen that the two patterns are orthogonal in polarization, with the exception of a small overlap in the *E*-phi components. Besides, angle diversity is achieved across the two antennas, since the directions of the peak gains are mostly complementary to each other. Therefore, the mutual coupling between the two ideal antennas is weak (S_{21} < -25 dB), despite the small center-to-center antenna separation of less than 0.15λ. Indeed, the pattern orthogonality of such a co-polarized dipole-loop antenna arrangement has been experimentally demonstrated in [16], though for the special case of co-located phase centers.

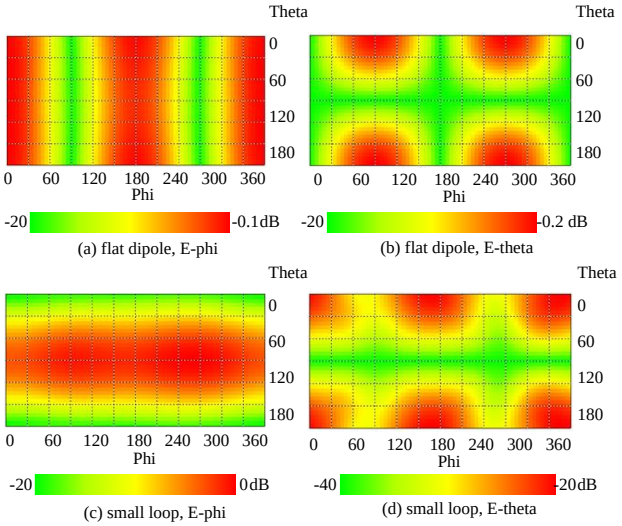

Fig. 3. The far-field radiation patterns for the flat dipole and the small loop at 0.9 GHz, normalized to the maximum field over both antennas.

In practice, however, the small loop in Fig. 2(a) cannot be directly used due to its small radiation resistance R_r of 0.045 Ω, which is calculated using the expression [17]

$$R_r = 20\pi^2 \left(\frac{C}{\lambda}\right)^4, \qquad (1)$$

where $C = 2\pi a$ is the circumference of the loop with radius a. The radiation efficiency of an antenna is determined by its radiation and loss resistances [17]. In general, the loss resistance of a single turn loop is much larger than its radiation resistance; thus the corresponding radiation efficiency is very low (< 10%). The ideal antenna study above assumes lossless material to ensure that the loop radiates efficiently. However, lossless material does not exist in reality. In addition, electrically small antennas also suffer from high Q factor and narrow bandwidth, as is evident in Fig. 2(b). The required matching network also complicates the design of the antennas system and introduces additional loss in reality. Thus, an efficient magnetic antenna with a much larger radiation resistance is desired. A normal way to increase the radiation resistance of the loop is to employ an *N*-turn loop, which unfortunately is difficult to implement on a planar PCB. In 2007, Erentok and Ziolkowski introduced a coupled feeding method for the loop, based on the idea of split ring resonator (SRR). The method effectively reduces the antenna dimension and increases the total efficiency [18], [19]. A more sophisticated 3D version was later proposed in [20]. In this paper, based on the antenna structure in [19], a planar coupled feed loop is employed to realize the magnetic antenna.

It is noted that the electric antenna at the chassis edge, which is used to excite the chassis, can also be moved to the center of the chassis. This alternative setup will still offer good isolation.

However, in this case, the chassis will function as a normal ground plane of the electric antenna and can no longer be efficiently excited as the radiator [12]. Since chassis excitation helps to increase the bandwidth (of the electric antenna) [21], such a strategy of avoiding chassis excitation is less desirable when considering performance in terms of both bandwidth and isolation. As for the magnetic antenna, since it is designed to not excite the chassis in order to achieve decoupling, its bandwidth is expected to be narrower than those of conventional terminal antennas, such as PIFAs and monopoles. Hence, in this paper, we focus on the case that an electric antenna is used to exploit chassis excitation in order to ensure a larger bandwidth, and a magnetic antenna is used to achieve good isolation in the presence of chassis excitation. Frequency reconfiguration will be applied to compensate the bandwidth limitation of the magnetic antenna in Section III-B.

III. Dual-Antenna System at a Low Frequency Band

A. Antenna Geometries and Performance

Based on the discussions in the previous section, a practical terminal antenna system consisting of a folded monopole (i.e., an "electric antenna") and a coupled feed small loop (i.e., a "magnetic antenna") is proposed. Folded monopoles are commonly used in mobile phones, due to their simplicity and good performance. The geometries of the antenna system are presented in Fig. 4(a). For ease of fabrication, the folded monopole and the coupled loop were printed on a thin copper layer above a substrate. The conductivity and thickness of the copper layer are 5.8×10^7 S/m and 35 μm, respectively. The substrate has a permittivity of 2.45, a loss tangent of 0.003 and a thickness of 0.8 mm. The monopole is fed by a microstrip line.

As observed from Fig. 4(a), the coupled feed small loop consists of two half square rings, with the inner ring acting as the matching feed and the outer ring as the main radiator. The inner ring is an impedance transformer, which transforms the port impedance (50 Ω) to the impedance of the outer loop. The outer half ring takes advantage of the shorter edge of the chassis to form a full ring, forming an efficient radiator. The simulated input resistance is around 42 Ω at the resonant frequency, which is almost a thousand-fold increase relative to that of the small loop in Fig. 2(a). Thus, high radiation efficiency is expected. The inter-digital capacitor, with both the arm width and inter-arm separation of 0.8 mm, is used to capacitively load the loop. The resonant frequency of the coupled loop can be tuned by the length of the arms (L_c) and the inter-arm separation.

It is noted that the feeding structure of the coupled loop is not limited to the half square ring. It can also be an inverted L-shape feed or a T-shape feed (see Figs. 4(b) and 4(c)), as long as it is an efficient impedance transformer to match the loop well.

The simulated S parameters of the dual-antenna system are shown in Fig. 5. It is observed that both the monopole and the coupled loop are well-matched, and the isolation is above 30 dB, which is very high for frequency bands below 1 GHz. Here, we note that the focus of this paper is on the new decoupling mechanism and its application on multiple antennas at low frequency bands. Therefore, we make no explicit effort to enlarge the bandwidth of the folded monopole.

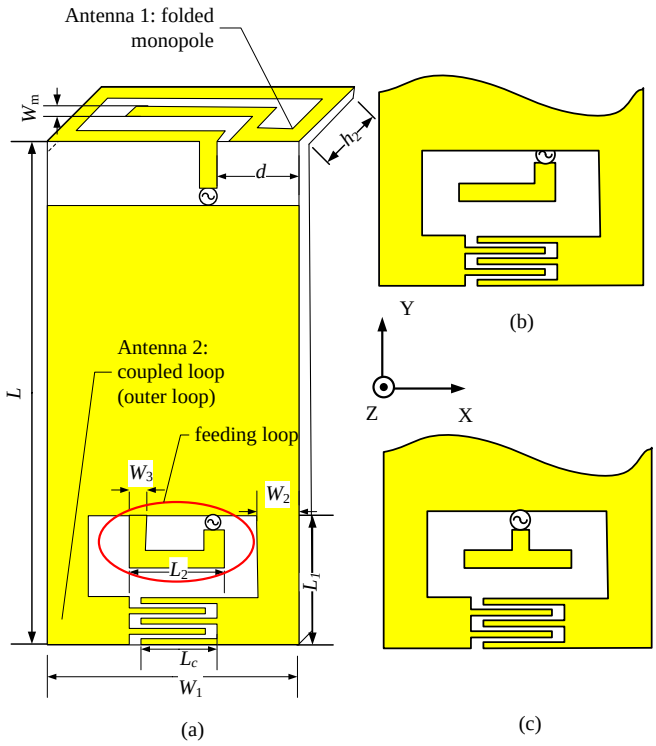

Fig. 4. (a) The geometries of the folded monopole and the coupled feed loop. The dimensions are: L = 100 mm, W_1 = 40 mm, L_1 = 15 mm, L_2 = 10 mm, h_2 = 6 mm, L_c = 7.5 mm, W_3= 2 mm, W_2 = 3 mm, W_m = 1 mm, d = 12 mm. (b) Coupled loop with inverted L-shape feed. (c) Coupled loop with T-shape feed.

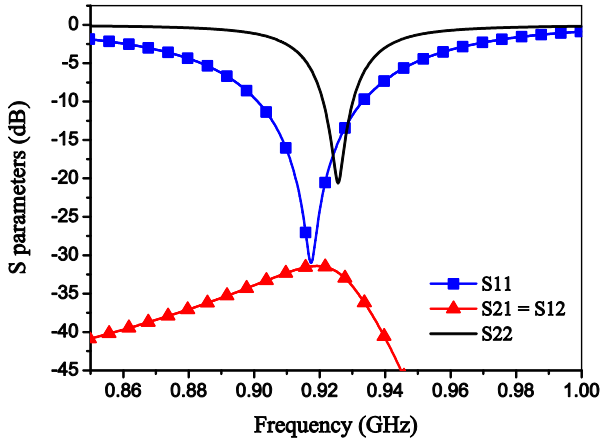

Fig. 5. The S parameters of the folded monopole and the coupled feed loop.

The total efficiency of an antenna ("antenna 1") in a two-antenna setup is given by $\eta_{total}= \eta_{rad}\,(1-|S_{11}|^2-|S_{21}|^2)$. Due to the high radiation efficiency η_{rad}, good matching ($|S_{11}|$, $|S_{22}|$ < -15 dB) and low mutual coupling ($|S_{21}|$, $|S_{12}|$ < -30 dB), the total efficiencies of both the monopole and the loop are very high, i.e., 92% and 80%, respectively, at 0.93 GHz.

In Fig. 6, the current distributions of the proposed antenna system are presented. As expected, Fig. 6(a) shows the strong chassis excitation by the monopole. From Fig. 6(b), it is observed that the current in the coupled loop (i.e., the outer loop) is almost constant when the loop is excited. Although the coupled loop makes use of the shorter edge of the chassis, the characteristic mode of the chassis is not excited. This

phenomenon is because the coupled loop radiates like a magnetic dipole, which as pointed out in Section II ensures good isolation from the monopole-induced chassis excitation.

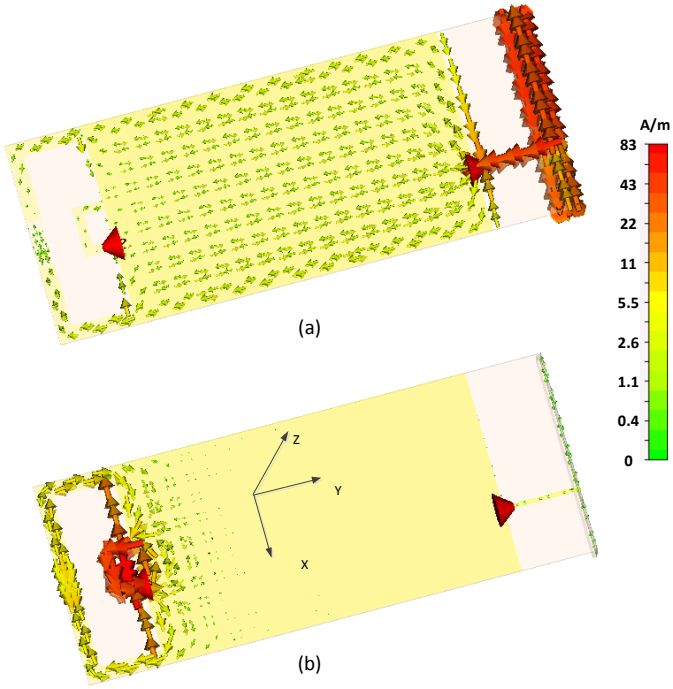

Fig. 6. The current distributions of the antenna system at 0.93 GHz (a) when the folded monopole is excited, and (b) when the coupled loop is excited.

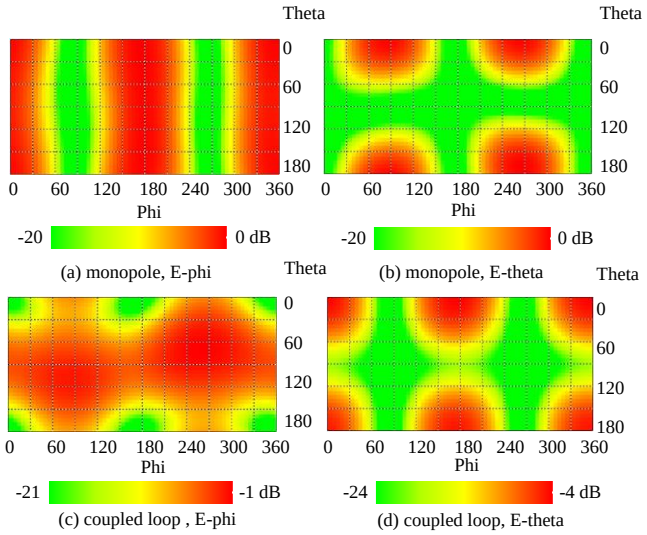

Fig. 7. The normalized far-field antenna patterns for the folded monopole and the coupled loop at 0.93 GHz.

The normalized far-field patterns of the proposed dual-antenna system are shown in Fig. 7. To ease comparison with Fig. 3, the *E*-theta and *E*-phi components are also separated. It can be seen that the radiation patterns of the proposed antennas largely mimic those of the ideal flat dipole and the small loop. This verifies that the chassis is the main radiator when the monopole is excited. The cross-polarization ratio (XPR) of the coupled loop antenna in Fig. 7 is smaller than that of the ideal small loop in Fig. 3. This is due to the increased loop dimension and the influence of the feeding. However, the *E*-phi component is still the main polarization, which is 3 dB larger than the *E*-theta component. The slight asymmetry in the *E*-phi component of the coupled loop is attributed to the asymmetric feeding method. Moreover, the patterns of the two antennas are still orthogonal in angle, contributing to low mutual coupling. The magnitude of the complex correlation coefficient calculated from the far-field patterns [22] is 0.003 at 0.93 GHz.

The effect of the human hand on the proposed dual-antenna system was also studied in simulation using a crude hand model. The simulated hand has a permittivity of 36.2 and an electric conductivity of 0.8 S/m. We found that the total efficiencies of the monopole and the coupled loop were reduced to 59% and 34%, respectively, when the hand was introduced. The isolation between antennas is still above 30 dB. The lower efficiency of the loop is partly due to more severe mismatch, which can be corrected using the reconfigurable setup proposed in Section III-B. The magnitude of the complex correlation is still below 0.1, indicating negligible impact of the correlation on system performance [22]. Comparing these numbers to conventional dual-antenna systems for the handheld case, such as the monopole-PIFA configuration in [11], the proposed structure gives significantly higher efficiency and low enough correlation to provide better system performance than conventional designs. A detailed study of user effect is left for future work.

B. Frequency Reconfigurable Coupled Loop

Compared with the folded monopole, the bandwidth of the coupled loop is narrow, as shown in Fig. 5. In this context, the folded monopole should be used as the main antenna, whereas the coupled loop can be used as a diversity antenna. This is because the diversity antenna may require a smaller operating bandwidth (e.g., only the receive band). In addition, the coupled loop can be made frequency reconfigurable via a simple modification: The inter-digital capacitor in between the two arms of the outer ring can be replaced by a varactor diode, as shown in the inset of Fig. 8. No matching network is needed. The resonant frequency of the loop can then be tuned by changing the capacitance value of the varactor. It is important to ensure that good impedance matching is maintained while the capacitance value varies over a large range. Therefore, as long as the bandwidth of the coupled loop for a given capacitance is larger than the signal bandwidth of the system of interest (e.g., up to 20 MHz for LTE), the covered bandwidth will only be limited by the tuning range of the coupled loop.

The S parameters of the coupled loop with different capacitance values are shown in Fig. 8. The loop can be continuously tuned, though for clarity of presentation only five capacitance values are illustrated. We noted that the frequency of the coupled loop can be tuned from 780 MHz to 980 MHz, covering a bandwidth of 200 MHz. The resonance of the monopole and the isolation performance between the antennas, which are not shown to avoid cluttering the figure, are largely unaffected by the tuning of the coupled loop. In practice, a tunable MEMS capacitor can be used instead of the varactor diode to reduce insertion loss [23].

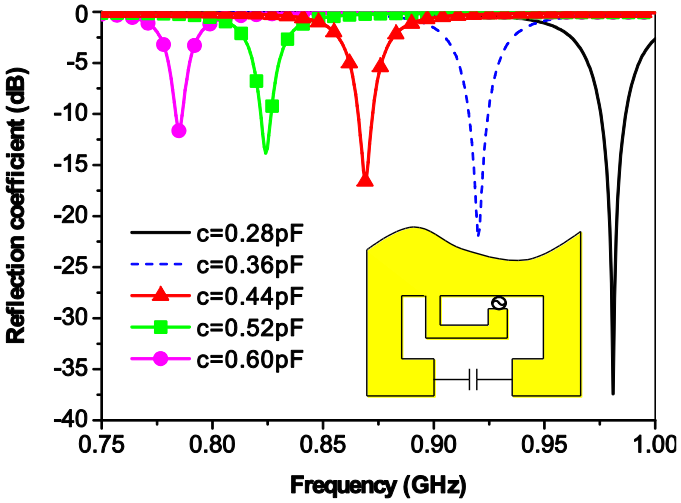

Fig. 8. The S parameters of the coupled loop, with different values of capacitance in between the two arms of the outer ring.

C. *Switchable Tri-band Dual Antenna System*

In this sub-section, the dual antenna system is designed practically to work in three bands, including the GSM900, GSM1800 and LTE2600 bands. The geometries of the dual-antenna system are presented in Fig. 9. In this case, the coupled loop is implemented on a hollow carrier made of plastic, which demonstrates the flexibility of the antenna structure to account for mobile phone integration. For example, a speaker and/or a camera can be placed inside the hollow carrier to facilitate better integration and conserve space.

The multi-resonance of the folded monopole is easy to create and tune by adding a short branch (L_{m2}) near its open end. For the coupled feed loop, three main modifications are needed to achieve multi-resonance. First, a switch is added to each of the outer ring and the inner ring, to switch the resonance(s) of the loop between the low band and the two higher bands. Second, a new branch (L_3) is added to the original structure to create high frequency resonances. Besides, the inner ring (feeding loop) is also modified in order to function as an efficient impedance transformer at the two high bands. When the two switches are on (short circuit), the structure of the loop is similar as that of the original loop in Section III-A, and it resonates at 0.93GHz. When the two switches are off (open circuit), the antenna radiates like a monopole. The lengths for the two different electrical paths of the antenna correspond to the frequency bands of 1.8 GHz and 2.6 GHz, respectively. The S parameters at the low band and the two higher bands of the dual antenna system are presented in Fig. 9(b) and 9(c), respectively. It can be seen that, through utilizing two switches, the three operating bands are fully covered by the dual antenna system, with an isolation of above 15 dB. The impedance matching at the higher frequency bands is mainly influenced by the width of the gap in the coupled feed (W_7), the length of the coupled feed (L_2) and the distance between the two antenna branches (d_1). When tuning these parameters, there is a trade-off between the impedance matching at 1.8 GHz and 2.6 GHz. Since the tri-band antenna system only serves to demonstrate the multiband potential of the proposed antenna as a practical consideration, and for the sake of conciseness, its working mechanisms and parameter analysis are not explained in detail here.

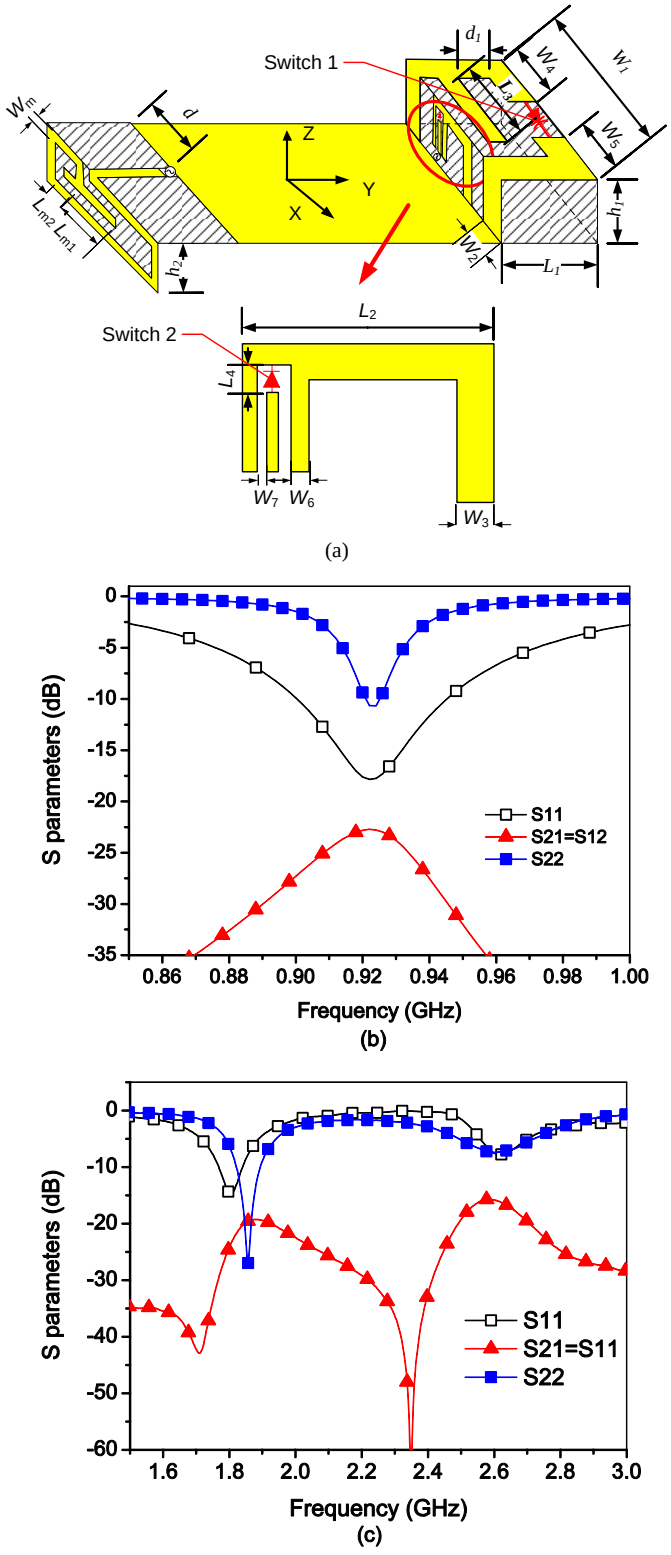

Fig. 9. (a) The geometries of the tri-band dual-antenna system. The dimensions are: L_1 = 17 mm, W_1 = 40 mm, L_2 = 14 mm, W_2 = 5 mm, W_3 = 2 mm, W_4 = 17mm, W_5 = 17 mm, W_6 = 0.5mm,W_7 = 0.3mm, L_3 = 22 mm, L_4 = 1.5 mm, h_1 = 6 mm, h_2 = 6 mm, d_1 = 5 mm, d = 12 mm, L_{m1} = 10 mm, W_m = 1 mm, L_{m2} = 5 mm. (b) The S parameters of the tri-band dual-antenna system at the low band, with switches on. (c) The S parameters at the higher bands, with switches off.

IV. Co-located Mobile Antennas

A. Decoupling Technique in Co-located Mobile Antennas

To reduce the space for antenna implementation on the chassis, the folded monopole and the coupled loop can be co-located on the same edge of the chassis, as presented in Fig. 10. The geometries of both antennas need to be slightly changed to ensure good impedance matching. However, achieving good isolation for this antenna setup is more challenging than in the previous case in Section III-A. This is because the feed points of the two antennas are very close to each other, and thus in general the coupling between the feeds results in a direct current path between the antennas, which degrades isolation.

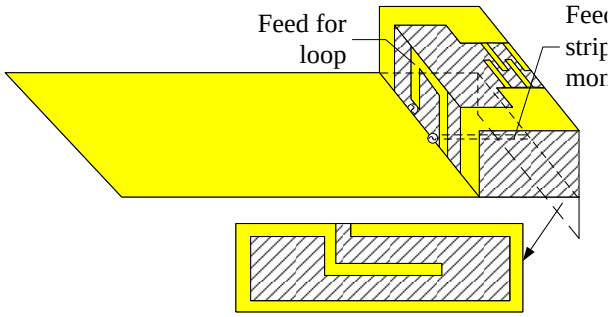

Fig. 10. The geometries of co-located dual-antenna system. The dimensions are: L_1 = 17 mm, W_1 = 40 mm, L_2 = 15 mm, W_2 = 7 mm, W_3 = 2 mm, h_1 = 6 mm, h_2 = 6 mm, L_c = 9.85 mm, d = 18.5 mm, L_m = 14.5 mm, W_m = 1 mm.

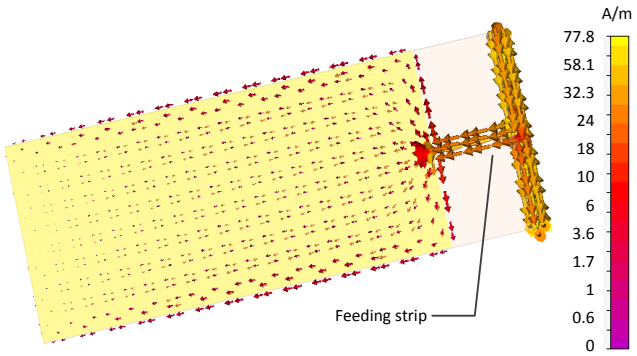

Fig. 11. The current distribution of the excited single folded monopole at the resonant frequency.

To solve the problem of coupling due to feed proximity, a single folded monopole antenna was studied first. The current distribution of the excited single folded monopole is presented in Fig. 11. It can be seen that the currents along the feeding strip are in phase when the monopole and the chassis are efficiently excited. To decouple the antennas in the dual-antenna case, we require the opposite situation of the currents along the feeding strip of monopole being out of phase when the coupled loop is excited. The near fields of the out-of-phase currents will then cancel one another and thus the monopole cannot be efficiently excited. The phases of the currents along the feeding strip are related to the electrical length of the current paths between the two feeds. Therefore, the coupling between the feeds critically depends on two parameters, namely, the length of the feeding of the small loop (L_2) and the location of the feeding strip of the folded monopole (d). However, any variation in L_2 will complicate the antenna design due to its strong influence on the impedance matching of the coupled loop. If L_2 is changed, other parameters, such as W_3 and L_c, need to be changed accordingly to ensure good impedance matching. Consequently, it is more convenient to optimize the location of the monopole's feeding strip in order to decouple the co-located antennas.

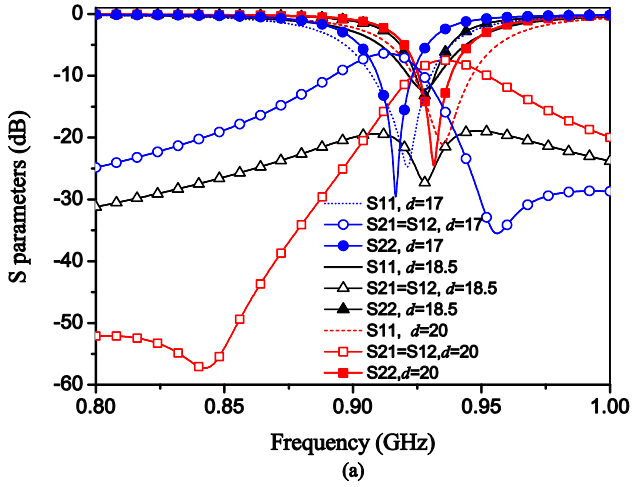

(a)

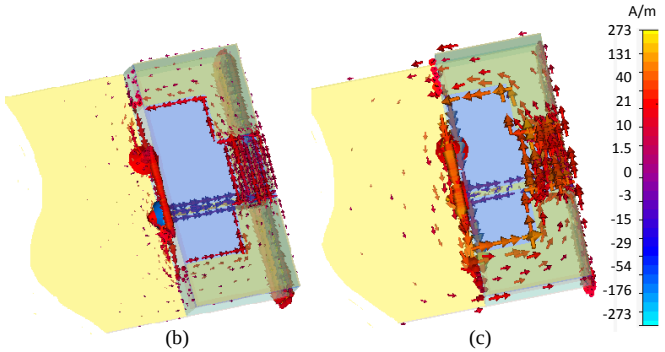

(b) (c)

Fig. 12. (a)The S parameters of the coupled loop, with different values of d. (b) the current distribution with d = 20 mm when the coupled loop is excited. (c) the current distribution with d = 18.5 mm when the coupled loop is excited.

The S parameters of the folded monopole and the coupled loop for three different values of d are presented in Fig. 12(a). From the figure, it is observed that when d = 18.5 mm, the isolation is over 20 dB for the whole operating band. However, in the other two cases, the isolations are below 10 dB. It is interesting to note that when the value of d changes, the frequency of the local coupling null (the minimum point of the "valley" in S_{21}) varies accordingly. This is explained as follows: The variation of d changes the physical length of the current path from the excited loop to the feeding strip of the monopole. Each physical length corresponds to different electrical lengths for the same frequency. There is one electric length satisfying the condition that the currents along the feeding strip are out of phase. The corresponding frequency is then the coupling null. For different physical lengths, the coupling null frequency will also be different. The isolation decreases as the frequencies depart from the frequency of the coupling null, thus forming the

shape of a valley. Figures 12(b) and 12(c) show the current distributions at 0.93 GHz for d = 20 mm and d = 18.5 mm, respectively, with only the loop excited. In Fig. 12(b), when d = 20 mm, the currents on the feeding strip of monopole are in phase. Therefore, the monopole is excited, and the coupling is severe. However, when d = 18.5 mm, the currents in Fig. 12(c) are out of phase on the feeding strip, forming a coupling null. In the optimization, the resonant frequencies of the two antennas and the frequency of the coupling null can be aligned. For ease of design, it is important that these frequencies can be tuned independently of one another. Indeed, these frequencies largely depend on the length of the monopole (L_m), the capacitance between the arms of the loop (L_c) and the location of the feeding strip (d), respectively. The decoupling method outlined above can also be applied to other multiple antenna systems, where the mutual coupling is caused by the proximity of the antenna feeds.

The total efficiencies when d = 18.5 mm are 80% and 76% for the folded monopole and the coupled loop, respectively. The total efficiencies of the co-located antennas are lower than antennas in Fig. 4(a), which is mainly the result of using the lossy hollow carrier, although poorer isolation is also a contributing factor.

B. MIMO Performance of the Co-located Mobile Antennas

Diversity gain and MIMO capacity are the most popular metrics for evaluating the performance of multiple antenna systems. Since the two metrics show similar trends, only capacity is presented in this paper. The capacity is calculated for different frequencies under the waterfilling (WF) condition [24] for a reference SNR of 20 dB. The WF procedure is performed over the antenna elements at each frequency. The Kronecker model [25] and uniform 3D angular power spectrum (APS) are assumed. There is no correlation between the (base station) transmit antennas, whereas the (terminal) receive antennas are correlated according to their patterns and the uniform 3D APS. The capacity is averaged over 10,000 identical and independently distributed (IID) Rayleigh realizations [24] at each frequency. The channels are normalized with respect to the IID Rayleigh case, which means that the correlation, total efficiency and efficiency imbalance are taken into account in the capacity evaluation.

The channel capacity for three cases are presented in Fig. 13, i.e., the IID Rayleigh channel, the proposed co-located dual-antenna system in uniform 3D APS, and a reference dual-antenna system in uniform 3D APS. The reference system is a typical monopole-and-PIFA configuration, with the two antennas located separately on the two shorter edges of the chassis [12]. The IID case corresponds to the ideal situation of 100% total antenna efficiencies and zero correlation between the antennas. The center frequency of the dual-antenna systems is 0.93 GHz. A bandwidth of 20 MHz is chosen because it covers the downlink bandwidth of a single LTE channel. From the figure, it is concluded that the proposed co-located antenna system not only saves implementation space on the PCB, but also increases the channel capacity by more than 2 bits/s/Hz, when compared to a typical dual-antenna design. If the two antennas are not co-located, as in Fig. 4, the channel capacity will further increase due to higher total antenna efficiencies.

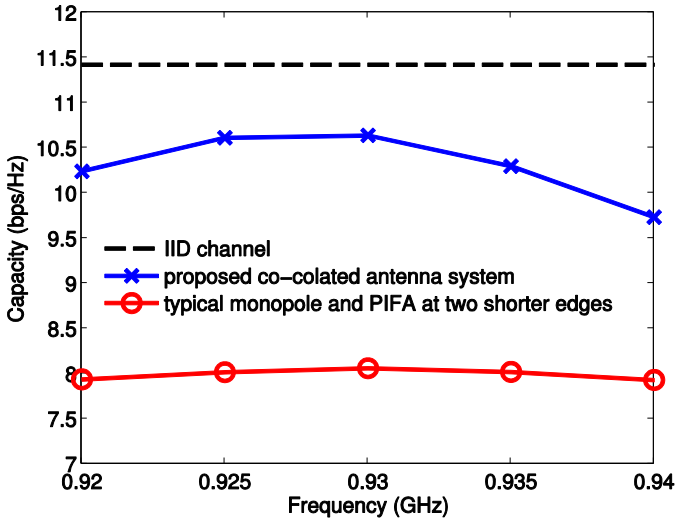

Fig. 13. Channel capacities for three different cases.

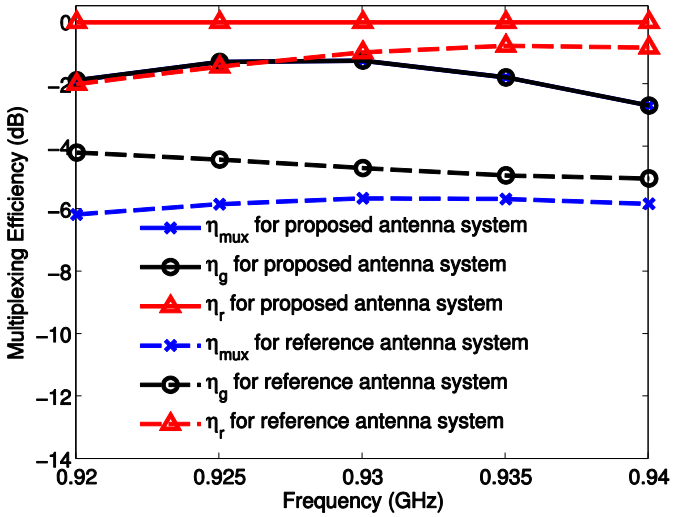

Fig. 14. Multiplexing efficiencies of the proposed and reference dual-antenna systems. η_{mux} and η_g for the proposed system almost overlap with each other.

In order to provide intuitive insights into the relative impact of different non-ideal effects of efficiency, efficiency imbalance and correlation on the capacity performance, we employ the multiplexing efficiency metric proposed in [26]. Multiplexing efficiency is the power penalty of a non-ideal antenna system in achieving a given capacity, relative to an ideal antenna system with 100% total antenna efficiencies and zero correlation. For a dual-antenna system, it is given by

$$\eta_{\text{mux}} = \underbrace{\sqrt{\eta_1 \eta_2}}_{\eta_g} \underbrace{\sqrt{(1-|r|^2)}}_{\eta_r}, \qquad (2)$$

where η_i is the total antenna efficiency of antenna i and r is the complex correlation coefficient in uniform 3D APS. The term η_g is the geometric mean (or geometric mean in decibel) of the antenna efficiencies, which shows the overall influence of efficiency and efficiency imbalance, whereas η_r reveals the equivalent power loss due to correlation. Fig. 14 illustrates η_{mux}, η_g and η_r for both the proposed and the reference dual-antenna

systems. It is observed that the multiplexing efficiency of the proposed antenna is around –2 dB at the center frequency, which is mainly attributed to practical limitations in antenna efficiency. The correlation coefficient of the proposed co-located antenna system is so small that its impact on the multiplexing efficiency (η_r) is negligible (~ 0 dB). As a result, η_g almost overlaps with η_{mux} for this case. On the other hand, the reference antenna system has a significantly lower multiplexing efficiency of –6 dB. The lower average antenna efficiency of the reference antenna setup [12] (–4 dB) contributes to a loss of 3dB in multiplexing efficiency with respect to that of the proposed antenna system. The high correlation is responsible for a further 1 dB loss, which can also be seen in the figure.

V. Experimental Results

The proposed co-located dual-antenna system in Section IV-A was fabricated and shown in Fig. 15. The SMA feeds of the two antennas are placed along the edge at the center of the chassis, as is typical for antenna mock-ups. The S parameters were measured with a vector network analyzer and shown in Fig. 16. It is observed that the isolation is above 20 dB in the operating band, though the coupling null deviates a little from the resonant frequency of the two antennas due to fabrication tolerance.

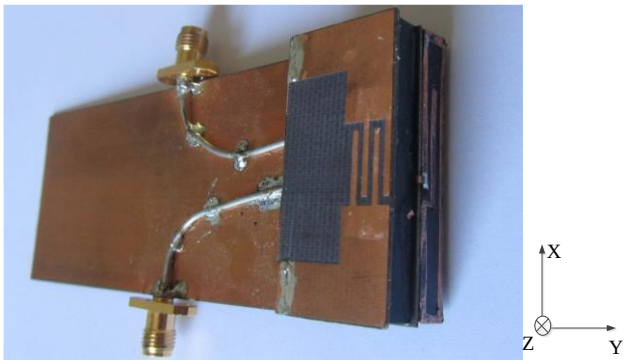

Fig. 15. The prototype of the co-located dual-antenna system, consisting of the folded monopole and the coupled loop.

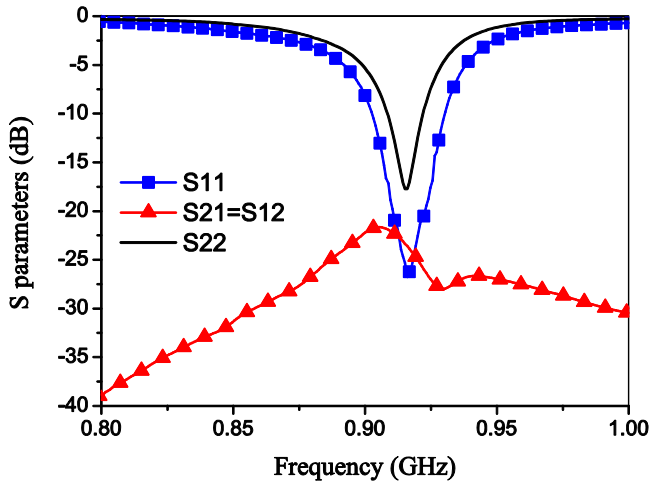

Fig. 16. The S parameters of the co-located antenna system.

The far-field patterns and efficiencies of the antenna were measured in a Satimo Stargate-64 antenna measurement facility. The measured patterns agree well with the simulated ones, as presented in Fig. 17. The slight differences are caused by the influences of the feed cables and the misalignment of the antenna resonant frequency and the coupling null. Due to the same reason, the correlation calculated from the measured patterns (0.1) is higher than that in the simulation (0.008). The measured efficiencies for the folded monopole and the coupled loop at 0.93 GHz are 71% and 66%, respectively, which are 9% and 10% lower than the simulated efficiencies. One reason for the efficiency drop is the additional resistive loss incurred in the thin feed cables as well as the solder joints in the fabricated antenna (see Fig. 15), especially the joints connecting the feed cables and the antenna structures. Moreover, during the pattern measurement, the antenna was supported by bulk foams with a loss tangent of 0.002, which introduce some losses. In addition, some differences between the actual and nominal loss tangents of the materials can also contribute to the discrepancy.

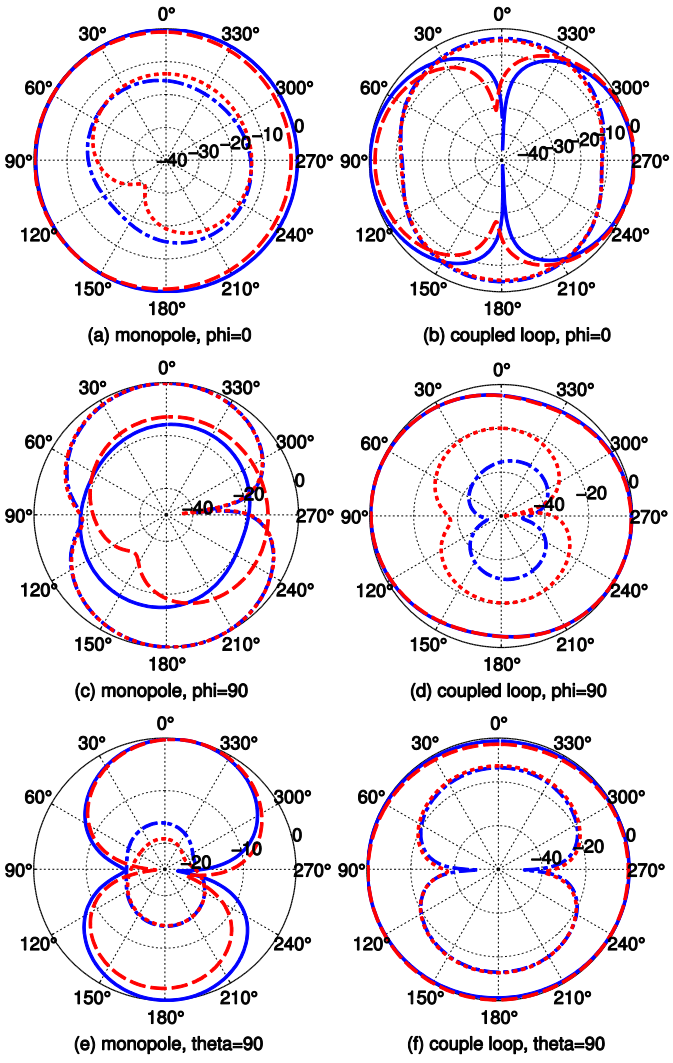

Fig. 17. Simulated and measured antenna patterns for the co-located antenna system: (——) measured *E*(theta), (– –) simulated *E*(theta), (– -)measured *E*(Phi), (--)simulated *E*(Phi).

VI. Conclusions

In this work, a novel concept for designing multiple antennas on small terminals was proposed. Specifically, for a dual-element design, an electric antenna is employed to exploit chassis excitation, whereas a magnetic antenna avoids such excitation to achieve good isolation performance. According to the concept, a folded monopole and a coupled loop is placed on opposite edges of a 100 mm × 40 mm chassis to form a practical dual-antenna design. The center frequency of both antennas is 0.93 GHz, and the isolation is above 30 dB within the operating band. In practice, the coupled loop can be made reconfigurable to cover a larger bandwidth of 200 MHz. In addition, both antennas can achieve multiband operation in the 900/1800/2600 MHz with minor modifications, including the addition of two switches. Furthermore, it is demonstrated that the two antennas can also be co-located on the same edge of the chassis, to conserve implementation space. By controlling the phase of the current on the monopole feed, the isolation of above 20 dB can be maintained for the entire operating band. A comparison between the co-located antenna and a typical monopole-PIFA design was carried out through channel capacity and multiplexing efficiency. It reveals that a significant capacity improvement of 2 bits/s/Hz is obtained by the proposed design for a reference SNR of 20 dB. The multiplexing efficiency also improves by 4 dB due to higher antenna efficiencies and lower correlation coefficients. This is despite the fact that the antennas in the reference monopole-PIFA design are not co-located. The co-located prototype was fabricated and measured, and the results were found to be in reasonable agreement with those from simulations.

Acknowledgment

The authors would like to thank Prof. Jørgen Bach Andersen of Aalborg University for helpful discussions.

References

[1] M. A. Jensen and J. W. Wallace, "A review of antennas and propagation for MIMO wireless communications," *IEEE Trans. Antennas and Propag.*, vol. 52, no. 11, pp. 2810-2824, Nov. 2004.

[2] B. K. Lau, "Multiple antenna terminals," in *MIMO: From Theory to Implementation*, C. Oestges, A. Sibille, and A. Zanella, Eds. San Diego: Academic Press, 2011, pp. 267-298.

[3] G. J. Foschini and M. J. Gans, "On limits of wireless communications in a fading environment when using multiple antennas," *Wireless Personal Commun.*, vol. 6, pp. 311-335, Mar. 1998.

[4] Z. Ying and D. Zhang, "Study of the mutual coupling, correlations and efficiency of two PIFA antennas on a small ground plane," in *Proc. IEEE Antennas Propagat. Soc. Int. Symp.*, Washington DC, Jul. 2005, pp. 305-308.

[5] B. K. Lau, J. B. Andersen, G. Kristensson, and A. F. Molisch, "Impact of matching network on bandwidth of compact antenna arrays," *IEEE Trans. Antennas Propag.*, vol. 54, no. 11, pp. 3225-3238, Nov. 2006.

[6] H. Li, J. Xiong, and S. He, "Extremely compact dual-band PIFAs for MIMO application," *Electron. Lett.*, vol. 45, no. 17, pp. 869-870, Aug. 2009.

[7] A. Diallo, C. Luxey, P. L. Thuc, R. Staraj, and G. Kossiavas, "Enhanced two-antenna structures for universal mobile telecommunications system diversity terminals," *IET Microw. Antennas Propag.*, vol. 2, no. 1, pp. 93-101, 2008.

[8] H. Li, J. Xiong and S. He, "Compact and low profile co-located MIMO antenna structure with polarization diversity and high port isolation," *Electron. Lett.*, vol.46, no. 2, pp.108-110, Jan. 2010.

[9] H. Li, J. Xiong, and S. He, "A compact planar MIMO antenna system of four elements with similar radiation characteristics and isolation structure," *IEEE Antennas Wireless Propag. Lett.*, vol. 8, pp. 1107-1110, 2009.

[10] Y. Gao, X. Chen, Z. Ying, and C. Parini, "Design and performance investigation of a dual-element PIFA array at 2.5GHz for MIMO terminal," *IEEE Trans. Antennas Propag.*, vol. 55, no. 12, pp. 3433-3441, Dec. 2007.

[11] V. Plicanic, B. K. Lau, A. Derneryd, and Z. Ying, "Actual diversity performance of a multiband antenna with hand and head effects," *IEEE Trans. Antennas Propag*., vol. 57, no. 5, pp. 1547-1556, May 2009.

[12] H. Li, Y. Tan, B. K. Lau, Z. Ying, and S. He, "Characteristic mode based tradeoff analysis of antenna-chassis interactions for multiple antenna terminals," *IEEE Trans. Antennas Propag.*,vol. 60, no, 2, pp. 409-502, Feb. 2012.

[13] U. Bulus, C. T. Famdie, and K. Solbach, "Equivalent circuit modeling of chassis radiator," in *Proc. German Microw. Conf. (GeMIC2009)*, Munich, Germany, Mar. 16-18, 2009.

[14] R. F. Harrington and J. R. Mautz, "Theory of characteristic modes for conducting bodies," *IEEE Trans. Antennas Propag*., vol. AP-19, no. 5, pp. 622-628, Sep. 1971.

[15] T. Svantesson, M. A. Jensen, and J. Wallace, "Analysis of electromagnetic field polarizations in multiantenna systems," *IEEE Trans. Wireless Commun.*, vol. 3, no. 2, pp. 641 – 646, Mar. 2004.

[16] D. Stancil, A. Berson, J. Van't Hof, R. Negi, S. Sheth, and P. Patel, "Doubling wireless channel capacity using co-polarised, co-located electric and magnetic dipoles," *Electron. Lett*., vol. 38, no. 14, pp. 746-747, Jul. 2002.

[17] C. A. Balanis, *Antenna Theory: Analysis and Design*, 2nd ed. CA:Wiley, 1997, pp. 78, 204-217, 523.

[18] A. Erentok and R. W. Ziolkowski, "An efficient metamaterial-inspired electrically-small antenna," *Microw. Opt. Tech. Lett*., vol. 49, no. 6, pp. 1287–1290, Jun. 2007.

[19] A. Erentok and R. W. Ziolkowski, "Metamaterial-inspired efficient electrically small antennas," *IEEE Trans. Antennas Propag*., vol. 56, no. 3, pp. 691–707, Mar. 2008.

[20] Y. Yu, J. Xiong, H. Li, and S. He, "An electrically small frequency reconfigurable antenna with a wide tuning range," *IEEE Antennas Wireless Propag. Lett.*, vol. 10, pp. 103-106, 2011.

[21] W. L. Schroeder, A. A. Vila, and C. Thome, "Extremely small wideband mobile phone antenna by inductive chassis mode coupling," in *Proc. 36th Europ. Microw. Conf.*, Manchester, UK, Sep. 10-15, 2006, pp. 1702-1705.

[22] R. Vaughan and J. B. Andersen, *Channels, Propagation and Antennas for Mobile Communications*. London, U. K.: IEE, 2003.

[23] G. M. Rebeiz, *RF MEMS Theory, Design, and Technology*, New York: Wiley, 2003.

[24] A. Paulraj, R. Nabar, and D. Gore, *Introduction to Space-time Wireless Communications*. Cambridge, U. K.: Cambridge University Press, 2003.

[25] J. P. Kermoal, L. Schmacher, K. I. Pedersen, P. E. Mogensen and F. Frederiksen, "A stochastic MIMO radio channel model with experimental validation," *IEEE J. Sel. Areas Commun.*, vol. 20, no. 6, pp. 1211-1226, Aug. 2002.

[26] R. Tian, B. K. Lau and Z. Ying, "Multiplexing efficiency of MIMO antennas," *IEEE Antennas Wireless Propag. Lett.*, vol. 10, pp. 183-186, 2011.